IAA-AAS-DyCoSS2-02-03

PERFORMANCE ANALYSIS OF REAL TIME PRECISE ORBIT DETERMINATION BY USING ADAPTIVE KALMAN FILTERING ON HIL GENERATED GPS RECEIVER DATA

Giuseppe Catastini and Francesco Menzione*

Currently on-board operating s/c navigation systems use Kalman filtering of GPS data to achieve real-time Precise Orbit Determination (POD). It allows to greatly reducing dependency on ground support, but high accuracy still relies on manual tuning from ground analysts. The suitable solution for this problem is the adaptive filtering approach. This paper presents the performance analysis of one POD adaptive Kalman filtering on Hardware-in-the-Loop (HIL) data generated by a dedicated GNSS facility. The study has demonstrated the capability of the innovation based adaptive filter to perform the self-tuning and improve the performance w.r.t. sub-optimal parameter initialization case.

INTRODUCTION

Nowadays almost all on-board operating spacecraft navigation systems use Kalman filter and Global Positioning System (GPS) data for the real time Precise Orbit Determination (POD) that is in charge to greatly reduce dependency on ground support and improve mission autonomy. The on-board orbit determination and prediction ensures great reliability w.r.t. ground station availability; it has also the potential to provide significant benefit when it will be integrated in the incoming autonomous orbit control systems.

The GPS sensor was gradually accepted as primary tracking system for real-time positioning and time-synchronization in spacecraft navigation when the kinematic method, or Standard Position Solution (SPS), was integrated in the framework of dynamic filtering. The solution, which is achieved by the sequential Kalman filtering of GPS measurement through the system model, ensures robustness against the rapid changing in the constellation viewing geometry due to spacecraft velocity. Currently, many receivers involved in space applications are equipped to provide a filtered solution: it allows reducing tracking loss by improving the availability of the service and the continuity of the PVT (Position Velocity and Time) solution.

Nevertheless, for applications where high precision geo-location is requested (SAR imaging, formation flying) many projects have preferred to develop and embark a dedicated navigation system capable to employ all the useful information for the on-board real time orbit determination task. The basic idea is to improve the navigation accuracy w.r.t. the embedded sensor solution, integrating GPS observables with a high fidelity s/c orbit propagator implemented by using the higher available computational resources. This is the well-known reduced dynamic approach[1] that

* Thales Alenia Space Italia S.p.A.

improves autonomy of the navigation system w.r.t. GPS information unavailability and allows employing the aiding techniques based on attitude and control input feed-forward, too.

As in the case of GEONS/TONS[2, 3] or GHOST[1], TAS-I has developed its navigation system, called POD system[4], which has demonstrated its reliability and efficiency in two different space mission programs with six flying satellites: the POD system interfaces the GPS receiver and it employs the standard solution as input.

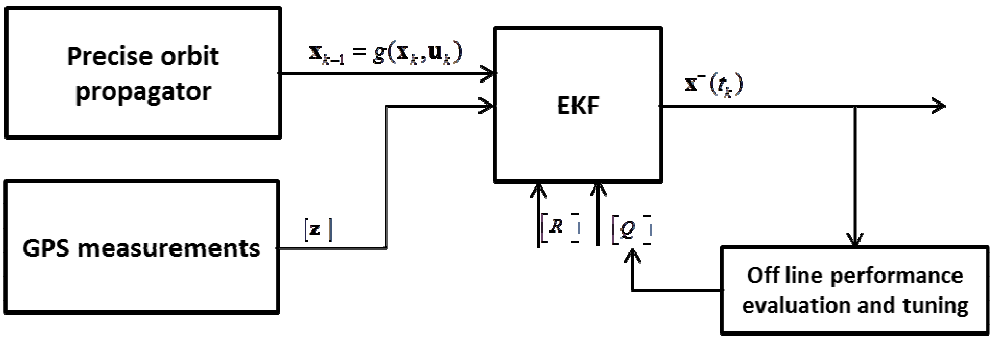

Figure 1. Standard POD system block diagram and tuning process

Even considering its robustness and efficiency, the perfect agreement between accuracy and autonomy of the system cannot be completely achieved because it still relies on time by time manual tuning from analysts (see Figure 1). The optimality is achieved only with the best design parameter set, which is often a few predictable and not constant all over the mission life time.

The solution proposed here is the adaptive filtering approach that allows estimating the noise covariance in order to ensure performance robustness vs. environmental or operational changes.

The aim of this work is demonstrating the real time applicability of the adaptive criteria within the TAS-I POD system by using HIL GPS data provided by a space qualified GPS receiver. Moreover, the adaptive approach has been tested on an enhanced POD architecture, also called tightly-coupled scheme, developed to deal with use of dual frequency pseudoranges and Doppler data. In this way the filter can be more precise and, as required, independent from SPS availability and capable to work in critical GNSS visibility conditions.

POD EXTENDED KALMAN FILTER DESIGN

Dynamics Model

The POD orbit propagator was developed in order to deal with the best compromise between accuracy and real time constraint. The motion of the satellite in the ECI reference frame is obtained by a step-wise 4rth order numerical integration of the continuous time model:

$$\begin{cases} \dfrac{d\,\mathbf{r}}{dt} = \dot{\mathbf{r}} \\ \dfrac{d\,\dot{\mathbf{r}}}{dt} = \mathbf{a}(\mathbf{r}, \dot{\mathbf{r}}, t) = \mathbf{P}_{grav} + \mathbf{P}_{drag} + \mathbf{P}_{thrust} \\ \mathbf{r}(t_0) = \mathbf{r}_0\,, \quad \dot{\mathbf{r}}(t_0) = \dot{\mathbf{r}}_0 \end{cases} \tag{1}$$

The gravitational contribution $\mathbf{P}_{grav}$ implements the EGM96 model and allows taking into account up to the 25th non-spherical perturbation degree and order. The drag model $\mathbf{P}_{drag}$ employs an analytic approximation of the modified Harris-Priester atmospheric model in order to reduce the computational load. The thrust $\mathbf{P}_{thrust}$ contribution is applied when in-orbit maneuvers are accomplished and the state model must be corrected by using the feed-forward of the control action.

The raw data processing takes into account the receiver clock bias and clock drift errors by integrating them in the state vector:

$$\mathbf{x} = \{\mathbf{r}, \dot{\mathbf{r}}, \Delta t, \Delta \dot{t}\} \tag{2}$$

and by propagating them in the framework of the state observer as a simple linear stochastic process. The augmented state estimation model becomes:

$$\dot{\mathbf{x}} = \mathbf{f}(\mathbf{x}(t), t) + \mathbf{w} = \begin{cases} \dfrac{d\ \mathbf{r}}{dt} = \dot{\mathbf{r}} + \mathbf{w}_r \\ \dfrac{d\ \dot{\mathbf{r}}}{dt} = \mathbf{a}(\mathbf{r}, \dot{\mathbf{r}}, t) + \mathbf{w}_{\dot{r}} \\ \dfrac{d\Delta t}{dt} = \Delta \dot{t} + w_{\Delta t} \\ \dfrac{d\Delta \dot{t}}{dt} = w_{\Delta \dot{t}} \end{cases} \tag{3}$$

The components of the state noise $\mathbf{w}$ are assumed to be uncorrelated Gaussian white-noise. In the error propagation task of the discrete process the transition matrix $\mathbf{\Phi}\ (t_{k+1}, t_k)$ must be computed at the current time, and so the numerical integration has to be applied to solve the system variational equation:

$$\dot{\mathbf{\Phi}}\ (t, t_k) = \mathbf{F}(\mathbf{x}, t)\mathbf{\Phi}\ (t, t_k) \tag{4}$$

where:

$$\mathbf{F}(\mathbf{x}, t) = \frac{\partial \mathbf{f}\ (\mathbf{x}\ , t)}{\partial \mathbf{x}} = \begin{bmatrix} [\varphi]_{6x6} & [0]_{6x2} \\ [0]_{2x6} & [C]_{2x2} \end{bmatrix} \tag{5}$$

is the Jacobian matrix derived from Eq. (1). It takes into account the analytic drag model and the terms of geopotential distribution up to J4 because this is sufficient to meet the targeted overall modeling accuracy. The model could be also augmented with un-modeled acceleration[1], but the configuration will be the standard one in order to exploit the adaptivity.

The models embedded in the POD orbit propagator allow computing time by time the transformation from the ECI reference frame, where the dynamics is computed, to the ECEF reference frame, where GPS satellite positions and velocities are expressed. The transformation is evaluated at each time step providing a linear relation between the two state vector representations:

$$\begin{Bmatrix}\mathbf{x}\\ \dot{\mathbf{x}}\end{Bmatrix}_{ECEF}=\begin{bmatrix}[R] & [0]\\ [\wedge\omega] & [R]\end{bmatrix}\begin{Bmatrix}\mathbf{x}\\ \dot{\mathbf{x}}\end{Bmatrix}_{ECI} \tag{6}$$

The transformation is complete, taking into account also the Earth's pole motion[3].

Measurement Model

The GPS raw data measurements employed by the developed precise orbit determination system are the pseudorange and Doppler observables derived from the code and carrier-phase measurement. Specifically, due to the availability of a GPS receiver equipped with dual frequency channels, the iono-free combination[5] of pseudoranges on L1 and L2 frequency is performed:

$$\rho_{IF}=2.54\rho_{L1}-1.54\rho_{L2} \tag{7}$$

The ionospheric path delay is compensated and the relationship between the raw measurement and the relative motion between the S/C and the constellation satellite can be expressed as follows:

$$\mathbf{z}=\mathbf{h}(\mathbf{x}(t),t)+\mathbf{v}=>\begin{cases}\tilde{\rho}_j=\left\|\mathbf{X}_j\left(t_j\right)-\mathbf{x}^r\left(t_R\right)\right\|+c\Delta t\left(t\right)+v_{j,\tilde{\rho}_j}\\ \dot{\tilde{\rho}}_j=<\left(\mathbf{V}_j\left(t_j\right)-\mathbf{v}^r\left(t_R\right)\right),\mathbf{e}_j>+c\Delta\dot{t}\left(t\right)+v_{j,\dot{\tilde{\rho}}}\end{cases} \tag{8}$$

where:

$$\mathbf{e}_j=\frac{\mathbf{X}_j\left(t_j\right)-\mathbf{x}^r\left(t_R\right)}{\left\|\mathbf{X}_j\left(t_j\right)-\mathbf{x}^r\left(t_R\right)\right\|} \tag{9}$$

$\tilde{\rho}_j$ is the iono-free pseudorange between the in view GPS satellite positioned in $\mathbf{X}_j\left(t_j\right)$ and the receiver hosted on board located at $\mathbf{x}^r\left(t_R\right)$, both expressed in ECEF reference frame. $\dot{\tilde{\rho}}_j$ is the Doppler measurement geometrically expressed as the relative ECEF velocities between GPS spacecraft and receiver, $\mathbf{V}_j\left(t_j\right)-\mathbf{v}^r\left(t_R\right)$, projected along the light of sight direction $\mathbf{e}_j$. Finally the components of the state noise $\mathbf{v}$ are assumed to be uncorrelated Gaussian white-noise.

This observation model set is used in the state estimation processing, and so the linearized equation model is evaluated as follow:

$$H_k=H(\mathbf{x},t)\Big|_{\mathbf{x}_k,t_k}=\frac{\partial\mathbf{h}(\mathbf{x},t)}{\partial\mathbf{x}}\Big|_{\mathbf{x}_k,t_k}=\begin{bmatrix}[E]_{nx3} & [0]_{nx3} & [1]_{nx1} & [0]_{nx1}\\ [\dot{E}\Delta V]_{nx3} & -[E]_{nx3} & [0]_{nx1} & [1]_{nx1}\end{bmatrix} \tag{10}$$

where $[E]_{nx3}$ indicates the direction cosine of the line of sight and $[\dot{E}\Delta V]_{nx3}$ represents the derivative of these direction cosines multiplied by the relative velocity.

When the SPS solution is available, the pseudorange and Doppler observables are corrected with the estimated clock bias and drift. It allows improving robustness of the filter thrusting on reduced augmented parameter excursion. When the SPS solution correction is not available the clock bias can be still estimated considering at that time an enhanced sigma for the clock process.

Estimation

The sequential optimal filtering of the presented navigation system is accomplished by using the Extended Kalman Filter (EKF), which is the most commonly adopted framework for non-linear estimation in real time application. The implemented discrete-time Kalman filter algorithm[6] can be summarized as follow:

Initialization:

$$\hat{\mathbf{x}}\ (t_0) = \hat{\mathbf{x}}_0\ ,\ P_0^- = E\left\{\mathbf{x}_0, \mathbf{x}_0\right\}$$

Correction:

$$K_k = P_k^- H_k^T \left[H_k P_k^- H_k^T + R_k\right]^{-1}$$

$$\nu_k = \mathbf{z}_k - \mathbf{h}\ (\mathbf{x}_k^-)$$

$$\mathbf{x}_k^+ = \mathbf{x}_k^- + K_k \nu_k$$

$$P_k^+ = \left[I - K_k H_k\right] P_k^- \left[I - K_k H_k\right]^T + K_k R_k K_k^T$$

$$H_k = \left.\frac{\partial \mathbf{h}\ (\mathbf{x}_k, t)}{\partial \mathbf{x}_k}\right|_{\mathbf{x}_k^-, t_k}$$

Prediction:

$$\mathbf{x}_i\ (t_{k+1}) = \mathbf{x}(t_k) + \int_{t_k}^{t_{k+1}} \mathbf{f}\left(\mathbf{x}(s), s\right) ds$$

$$P_{k+1}^- = \Phi_k P_k^+ \Phi_k^T + Q_k$$

$$F_k = \left.\frac{\partial \mathbf{f}\ (\mathbf{x}_k, t)}{\partial \mathbf{x}_k}\right|_{\mathbf{x}_k^+, t_k} \xrightarrow{(4)} \Phi_k \qquad (11)$$

where:

$$\begin{cases} E\{\mathbf{w}_k, \mathbf{w}_j^T\} = Q_k \delta_{kj} \\ E\{\mathbf{v}_k, \mathbf{v}_j^T\} = R_k \delta_{kj} \\ E\{\mathbf{w}_k, \mathbf{v}_k^T\} = 0 \end{cases}$$

It should be noted that the measurement matrix dimensions, in case of the highly coupled solution, are time variant due to the number of visible GPS satellite employed in the PVT evaluation. The following procedure is implemented:

$$R_{t_{k+1}} = P_{reord} R_{t_k} P_{reord}{}^T, \qquad \sigma^2{}_{\nu_j, new} = \sigma^2{}_{\nu_j, 0} \qquad (12)$$

where P_{reord} is the permutation matrix based on satellite identifiers and $\sigma^2{}_{\nu_j, new}$, which is the sigma of the new GPS satellite tracked at current epoch, is fixed at the reference noise level of the measurement $\sigma^2{}_{\nu_j, 0}$.

Finally, it shall be noted that the linearization point and the Jacobian matrix of state and prediction models are expressed in two different reference frames. Thus, in order to provide a right prediction-correction operating cycle, the following linear map is derived from transformation defined in Eq. (6):

$$M = \begin{bmatrix} [T] & [0] \\ [0] & [I] \end{bmatrix} \qquad T = \begin{bmatrix} [R] & [0] \\ [\wedge \omega] & [R] \end{bmatrix} \qquad (13)$$

This map is used in order to convert not only the state but also the matrices involved in the estimation process.

ADAPTIVE APPROACH

The optimality of Kalman filter relies on the level of knowledge of the process noise covariance matrix Q and of the measurements noise covariance R[7]. The performance is so sensitive vs. the measurement and process noise, that test analyses are usually foreseen in order to accomplish filter tuning. Actually, an error on these parameters not only affects the performance but it could lead to filter divergence.

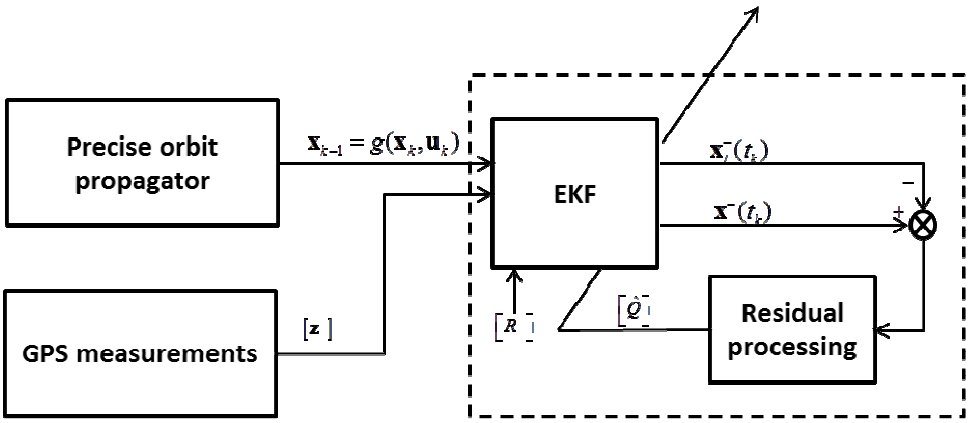

Figure 2. Adaptive Extended Kalman Filter block diagram.

Many algorithms for the adaptive estimate of the covariance matrices have been presented. One type of algorithms is based on multiple model adaptive estimation (MMAE) in which it is assumed that the system obeys one of a finite number of models[8]; other types are the state residual or the measurement innovation based estimation algorithms (RAE, IAE) in which state residual or measurement innovation are used to estimate the process and measurement noise statistics[9]. The MMAE is time-consuming and takes heavy computation burden, so the real time reliability makes the focus on innovation based approach. Maybeck categorized these approaches as: maximum likelihood[10], correlation and covariance matching methods[11].

In this work the first one is investigated. The reduced maximum likelihood equation with a finite window of length N for adaptive covariance Kalman filter[10] is:

$$\sum_{j=j_0}^{k} tr\left\{\left[A(t_j)^{-1} + A(t_j)^{-1}\nu_j\nu_j^T A(t_j)^{-1}\right]\frac{\partial A(t_j)}{\partial \alpha_{ii}}\right\} = 0 \qquad j_0 = k - N + 1$$
$$A(t_j) = \left[H(t_j)P_k^-(t_j)H(t_j) + R_k(t_j)\right] \tag{14}$$

Choosing α_{ii} as an element of the process or of the measurement covariance, an unbiased estimator can be obtained. Adaptation of both covariance can be very dangerous because it could cause divergence[7] without well-posed conditions. In this work the Q adaptation (see Figure 2) is implemented because the knowledge of the sensor noise is usually better than the knowledge of the process noise w.r.t. real environmental conditions. Thus putting $\alpha_{ij} = \sigma_{w_{ij}}$ in Eq. (14) the maximum likelihood estimator of process covariance for the on-line application can be derived:

$$\hat{Q} = \frac{1}{N}\sum_{j=j_0}^{k} \Delta x(t_j)\Delta x(t_j)^T + P^+(t_j) - (P^-(t_j) - Q\ (t_j))$$
$$\Delta x(t_j) = x_j^{\ +} - x_j^{\ -} \tag{15}$$

In order to reduce the computational cost of the on-line adaptation scheme only the diagonal elements of Q are estimated; details on the moving average window length N will be given in the dedicated section (window size comparison).

Eq. (16) cannot be applied as is but it needs same modifications. Actually, many applications[7] simplify it considering the predicted residual covariance negligible when steady state is achieved. In tightly-coupled application[15] the non-stationary variation of gain and covariance due to the GNSS scenario evolution doesn't allow to use the reduced formula. Moreover, it introduces other difficulties because the complete estimator has the potential limitation to not guarantee the process noise estimate to be positive definite[13]. The following schemes can be selected:

1)
$$\hat{Q} = \begin{cases} Q^* = \frac{1}{N}\sum_{j=j_0}^{k} \Delta x_j \Delta x_j^{\ T} + P_j^+ - (P_j^- - Q_j), & Q^* > 0 \\ Q_k, & Q^* \le 0 \end{cases} \tag{16}$$

2)
$$\hat{Q} = \begin{cases} Q^* = \frac{1}{N}\sum_{j=j_0}^{k} \Delta x_j \Delta x_j^{\ T} + P_j^+ - (P_j^- - Q_j), & Q^* > 0 \\ Q_k + \frac{1}{N}\cdot(\tilde{Q} - Q_k), \quad \tilde{Q} = (\Delta x_k \Delta x_k^{\ T} - P_k^+ + (P_k^- - Q_k)) & Q^* < 0 \end{cases} \tag{17}$$

where $\hat{Q}$ represents the estimation of process noise covariance at current time t_k. This value is propagated at next step by using:

$$\hat{Q}_{k+1} = \int_{t_k}^{t_{k+1}} \Phi(t_{k+1}, s) Q(s) \Phi(t_{k+1}, s) ds \qquad Q(s) = \hat{Q} / \Delta t \tag{18}$$

Eq. (18) derives the discrete time covariance from its continuous value by solving it at each step with the procedure described by Von Loan[12].

The first scheme ensures the covariance to be positive defined by simply holding it on the last estimated value. The second scheme implements, when the reference formula cannot provide a valid solution, the modified version of the estimator proposed by Busse[15]. This biased estimator allows obtaining a positive defined solution.

When the tightly-coupled approach is used with real data, it is also suitable to avoid the "washing-out"[14] effect due to the clock noise on the uncertainty in the vehicle dynamics. Several tests with HIL data have demonstrated the capacity of the developed adaptive filter to estimate the entire state vector; they have also focused that problems can occur if the first guess values and other filter parameters are chosen too far from the realistic ones. The problem can be overcome

by holding at a constant value either the dynamics or the time partition. This solution makes the filter more robust and allows a sensitivity analysis and performance comparison within a wide range of wrong starting values.

In this application a constant clock noise solution is chosen, too: in this way six adaptive degrees of freedom are available and only two parameters shall be set a priori. By adopting this solution the time parameters can be easily derived from the receiver characteristics and from the expected measurement bias. Generally, even if a wrong choice of the fixed time covariance can affect the final accuracy, the overall performance is better than choosing a fixed dynamics covariance (and adapting the time one).

TEST BENCH

The GNSS receiver measurements used to feed the Adaptive Kalman Filter are provided by a flight GPS Receiver mounted on one TAS-I Avionic Test Bench. The Avionics Test Bench is in charge of providing the required facilities to support the testing activities, from the functional point of view, of its dedicated satellite Avionics subsystem.

The main functions performed by the Avionics Test Bench are: providing the simulation of the necessary power, providing the simulation of the Telemetry/Telecommand link, providing the I/F for the external HL command acquisition, providing the simulation of all the external HW I/F, providing the real-time closed loop simulation capability at BUS 1553 level, providing the facility to support the real-time simulation of satellite dynamics, providing a Central Checkout System.

Figure 3 provides a schematic representation of the Avionics Test Bench architecture. It is split in the following functional blocks:

- a Central Checkout System (CCS) consisting on: 1 Computer to run Master Test Processor (MTP), Test Conductor Console (TCC), and to provide Data Storage and off-line processing capabilities
- LAN connecting the CCS with all the EGSE equipment
- a Power Simulation FEE (PWR FEE)
- a Satellite Housekeeping FEE (SLHK)
- an AOC FEE
- a Telemetry/Telecommand FEE (TM/TC FEE), with HL command acquisition capability
- a Spacecraft Management Unit (SMU) flight model
- a 1553 & SpaceWire FEE able to simulate all the Bus 1553 Remote Terminals and to acquire the data traffic from/to real Remote Terminals connected on the bus in real-lime closed loop tests and also to acquire and store SpaceWire data flow
- a Spark CPU to run the real-time Dynamics Simulation SW (DSS)
- a very high speed optic fiber interconnection network (Reflective Memory loop) to support DSS in real-time closed loop simulation capability

The Avionics Test Bench includes also the additional unit-custom special FEE's, in particular the Star Tracker EGSE, and the relevant EGSE for the test of the Adaptive Kalman Filter:

- a GPS Constellation multi-channel HW Simulator, connected to the GPS-R RF input, and integrated in the Avionics Test Bench through the LAN network with its host computer

Figure 4 shows the GPS Constellation Simulator (dedicated HW) with its host computer and its application SW.

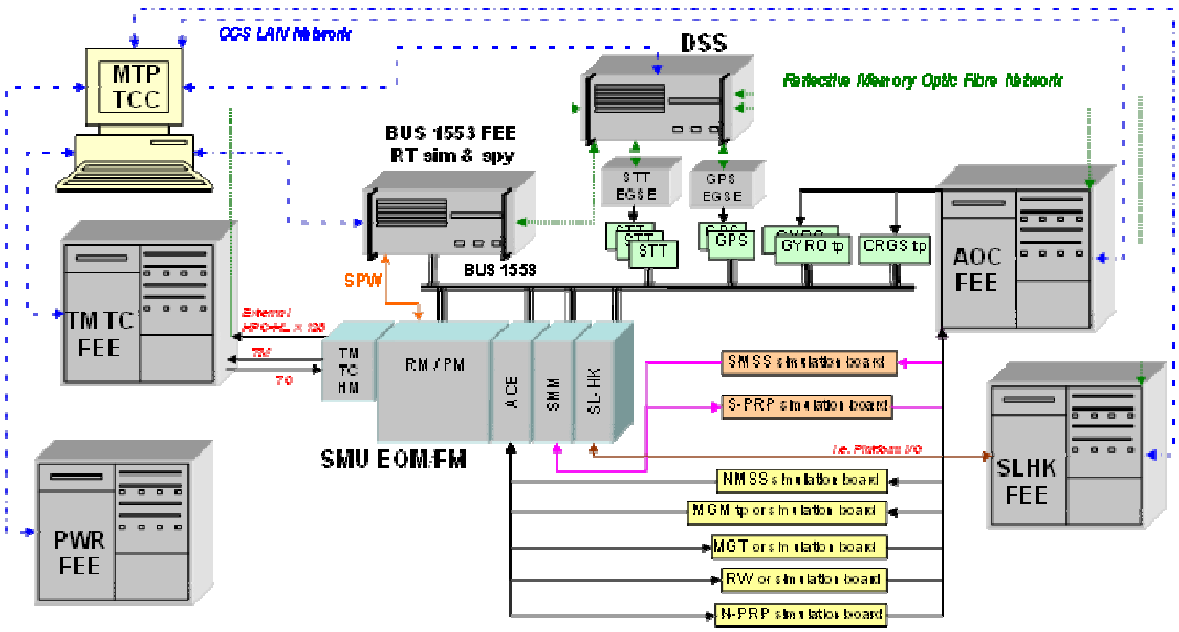

Figure 3. Avionics Test Bench block diagram

The GPS Constellation HW Simulator and its host computer are in charge of feeding the GPS-R RF input with the signals of the GPS constellation space vehicles in the field of view of the receiver's antenna, epoch by epoch.

Figure 4. GPS Constellation Simulator

The real-time chain "Dynamics Simulation SW – GPS EGSE – GPS Receiver" works according to the following logic flow:

- the DSS provides through an Ethernet connection the following data to the computer hosting the GPS Constellation Simulator SW application @8 Hz: time stamp, mot command, vehicle (hosting the GPS receiver) identifier, CoG vehicle position (x, y, z), CoG vehicle velocity (x, y, z), CoG vehicle acceleration (x, y, z), CoG vehicle jerk (x, y, z), vehicle attitude (heading, elevation, bank), vehicle angular rate (x, y, z), vehicle angular acceleration (x, y, z), vehicle angular jerk (x, y, z)

- the GPS Constellation Simulator SW application propagates the GPS constellation to the current epoch and, on the basis of the position, velocity, attitude and angular rate of the s/c hosting the GPS receiver, computes the L1 and L2 signals to be synthesized by the GPS Constellation multi-channel HW Simulator
- the GPS Constellation HW Simulator synthetizes the RF signals according to its SW application command and feeds the GPS receiver input (antenna)
- the GPS receiver telemetry output is sent (through the Bus 1553) to the on board computer (SMU) for the real time AOC purposes (Precise Orbit Determination) and to the Master Test Processor (through the TM/TC FEE)

The received GPS receiver telemetry and the SimGen commanded orbit are then post processed in order to provide the GPS-R measurements in engineering units and the satellite "true"(from dynamics) orbit (ECEF spacecraft position and velocity, antenna geometric center position and velocity in ECEF) and attitude.

DATA AND TEST ANALYSIS

GNSS Scenario

Two different scenarios for the generation of HIL data have been considered, in order to verify the AKF vs. EKF performance with different environmental conditions, different time series of GPS satellites geometry, and different duration of the time span for the data acquisition. The different duration for the two scenarios has been chosen to demonstrate the AKF (and EKF) capability of providing a stable performance.

The two available sets of HIL data are spanning 9680s and 24000s respectively. They refer to the same reference orbit scenario (summarized in Table 1) on two different dates (2011/06/21 01:16:00 and 05:32:11 in UTC time).

Table 1. Orbit and dynamics parameters setting.

Orbit Properties: LEO solar-synchronous orbit initial conditions $\{a, e, i, \Omega, \omega, \nu\} = \{7080147.3480, 0.0012, 98.1123, 249.6649, 68.9302, 291.0928\}$
Dynamics Model: • GEM10 Geopotential model (30x30) • Atmospheric Drag (Jacchia 1976), IGRF-10 Earth magnetic field • Solar Radiation Pressure with eclipse model • Luni-Solar perturbation
S/C properties: $\{mass,\ f.area, l.area, Cd, Cr\} = \{2139\text{kg}, 5.44\text{m}^2, 32\text{m}^2, 0, 0\}$ $\{mass,\ f.area, l.area, Cd, Cr\} = \{2139\text{kg}, 5.44\text{m}^2, 32\text{m}^2, 2.25, 1.3\}$ The satellite is assumed controlled on the three axes with nadir pointing reference attitude

Figure 5 and Figure 6 show the receiver SPS performances. The first dataset provides a SPS 3D position error of 2.60 m with a mean GDOP of 3; the second dataset provides a SPS 3D position error of 2.83m with a mean GDOP of 3.3: the long period simulation exhibits a slightly bigger amplitude error at orbit frequency.

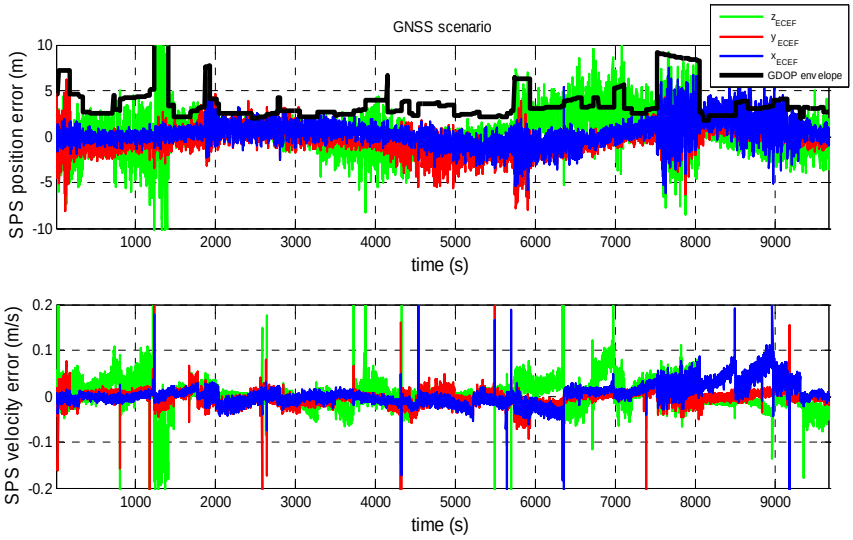

Figure 5. GPS SPS performance for the 1th GNSS scenario dataset.

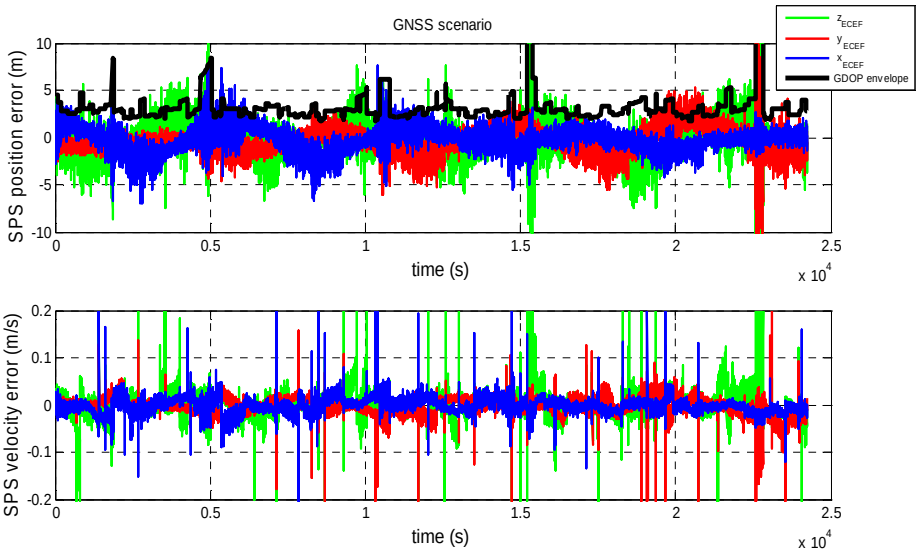

Figure 6. GPS SPS performance for the 2th GNSS scenario dataset.

We remind here that the contribution to the gravity field (disturbing term) due to the order and degree higher than 25 is provided by the Kaula's rule of thumb[17]. The overall contribution of the l-order and degree of the harmonic spherical expansion of the Earth geopotential is provided by:

$$\Delta g_l = \frac{GM_\oplus}{r^2} \cdot (l+1) \cdot \sigma_l$$

with $\sigma_l = \sqrt{\sum_{m=0}^{l} \left(C_{lm}^2 + S_{lm}^2\right)} \cong \frac{10^{-5}}{l^2} \cdot \sqrt{(2l+1)}$, i.e. $\Delta g_l = 2.3 \cdot 10^{-5}\, m/s^2$ for l=26. The cumulative disturbing effect due to the contribution from 26th to 30th order and degree is $\Delta g = 5 \cdot 10^{-5}$ m/s^2, i.e. less than 1 mm in 1 sec of orbit integration. Actually the main gravity "error" is due to

the difference in the low harmonics of the geopotential model between "true" dynamics and POD orbit propagator, and not on the truncation of the POD gravity field harmonics content (as it happens in flight).

Filter setting

The filter operating cycle is 1s in order to process 1Hz pseudoranges and Doppler measurements. The following filter noise properties are considered for both tests:

- GPSR measurement noise:
  $\sigma^2_{\nu_{\tilde{\rho}_j}} = 0.5(m^2), \qquad \sigma^2_{\nu_{\dot{\tilde{\rho}}_j}} = 0.008(m^2/s^2) \qquad j = 1 \ldots m$
- Dynamic process noise:
  $\sigma^2_{0\,\mathbf{w}_r} = 10(m^2) \quad \sigma^2_{0\,\mathbf{w}_{\dot{r}}} = 0.1(m^2/s^2) \quad \sigma^2_{w_{\Delta t}} = 100(m^2), \qquad \sigma^2_{w_{\Delta \dot{t}}} = 0.4(m^2)$

The value of the measurement noise results slightly conservative w.r.t. the receiver nominal performances. It takes into account un-modeled errors on the test bench and receiver configuration. This choice is also suitable because it allows to be more robust w.r.t. measurement accuracy discontinuity due to rapid changing in geometrical condition and number of visible satellites.

As regard the process noise, the position and velocity σ_0^2 represent the maximum reference value. The first guess values for the adaptive filter are derived from these maximum values by multiplying them by a scale factor α. In this way the initial conditions can be changed continuously: a sensitivity analysis is provided in the following section.

EKF/AKF comparison

In this section the canonical and adaptive Kalman filters are compared. The adaptive Kalman filter is started after exhaustion of the residual convergence transient, which occurs at t=2000s. A window length of N=10 is selected for adaptation.

The EKF vs. AKF comparison relies on the following procedure. The EKF and the AKF are executed within an α parameter loop, which defines the first guess variance value for the AKF and the constant variance value for the EKF:

- $-10 \le \log_{10}(\alpha_i) \le 0$
- $\sigma_i^2 = \alpha_i \cdot \sigma_0^2$

Each run of the AKF and EKF for a fixed value of α provides a vector with six std error components. Figure 7 and Figure 9 show the time series of the first scenario position and velocity errors of the EKF and AKF filters for a fixed value of the α parameter (over-estimated first guess σ). It is noticeable that the AKF error is (as expected) by far less that the EKF error.

Figure 8 and Figure 10 show the std of the first scenario position and velocity errors of the two filtering methods vs. the α parameter value. It is noticeable that the AKF performance is almost flat all over the α values range. The EKF performance is instead highly sensitive to the α parameter value: it achieves the best performance in a narrow range of the α parameter (variance setting). The best performance achieved by the AKF is almost tangent to the EKF minimal std error (optimal tuning). Figure 8 and Figure 10 point out that the AKF converges for each value of α (i.e. for each first guess variance) and that it converges to a value which is very close to the optimal one.

Figure 11, Figure 13, Figure 12 and Figure 14 confirm that the above described AKF properties are stable for very long time span, provided by the second scenario dataset.

As expected, the AKF keeps the same sub-meter 3D rms performance provided by the optimally tuned EKF in both scenarios.

1st Scenario

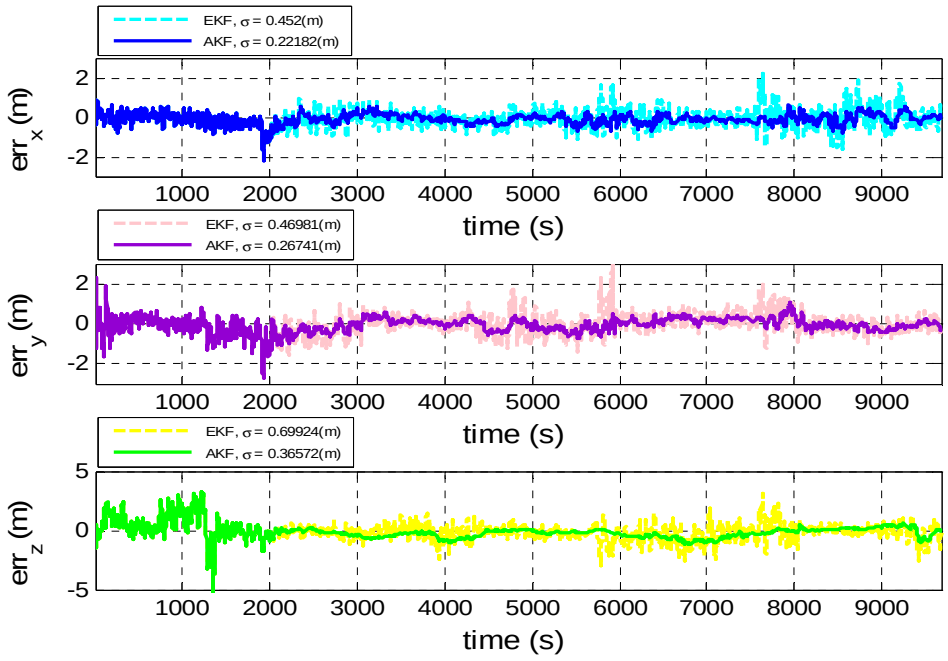

Figure 7. ECEF position error for EKF and AKF computed with $\alpha^{1/2}$=0.02 (1st scenario).

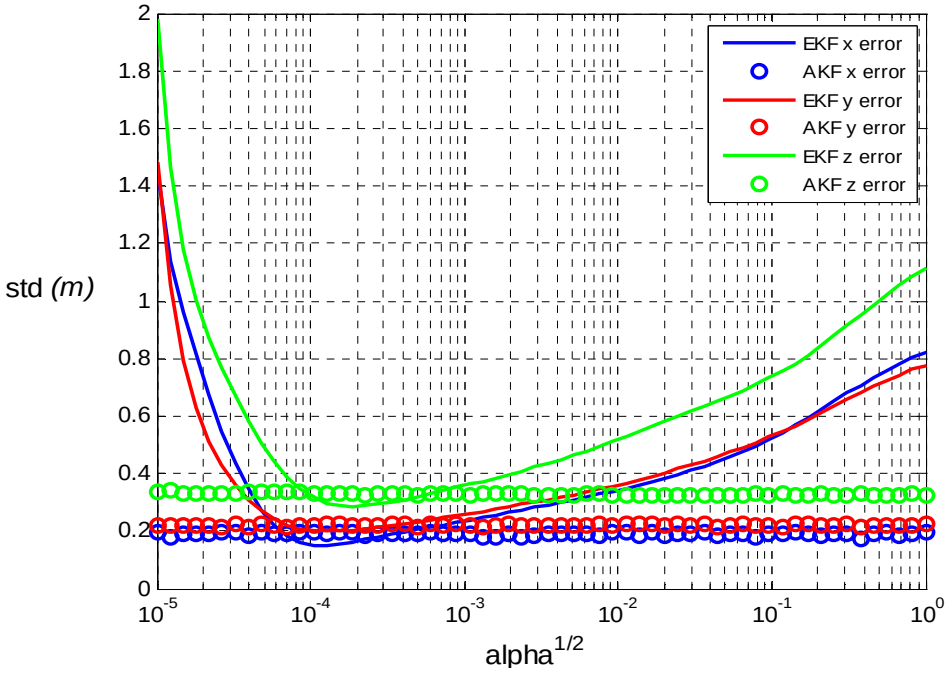

Figure 8. EKF and AKF position error std vs. $\alpha^{1/2}$ value (first guess setting).

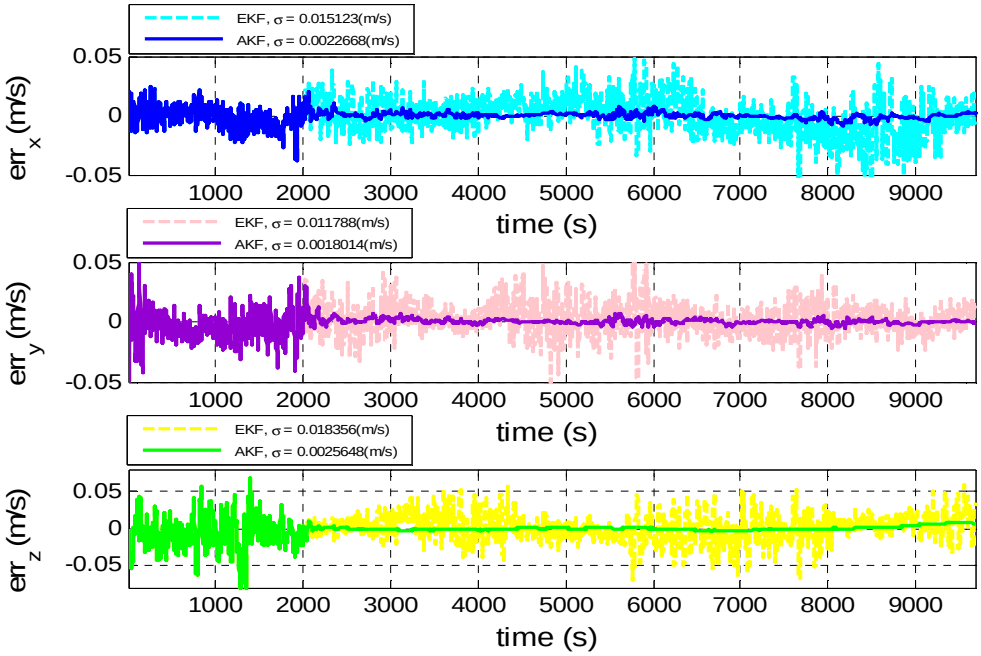

Figure 9. ECEF velocity error for EKF and AKF computed with $\alpha^{1/2}$=0.02 (1st scenario).

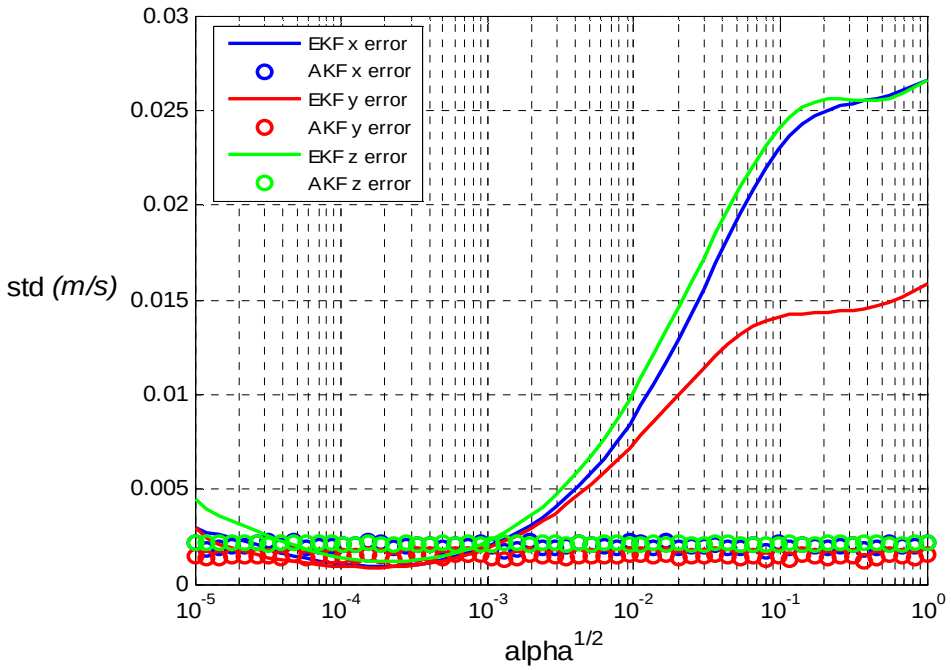

Figure 10. EKF and AKF position error std vs. $\alpha^{1/2}$ value (first guess setting).

2nd Scenario

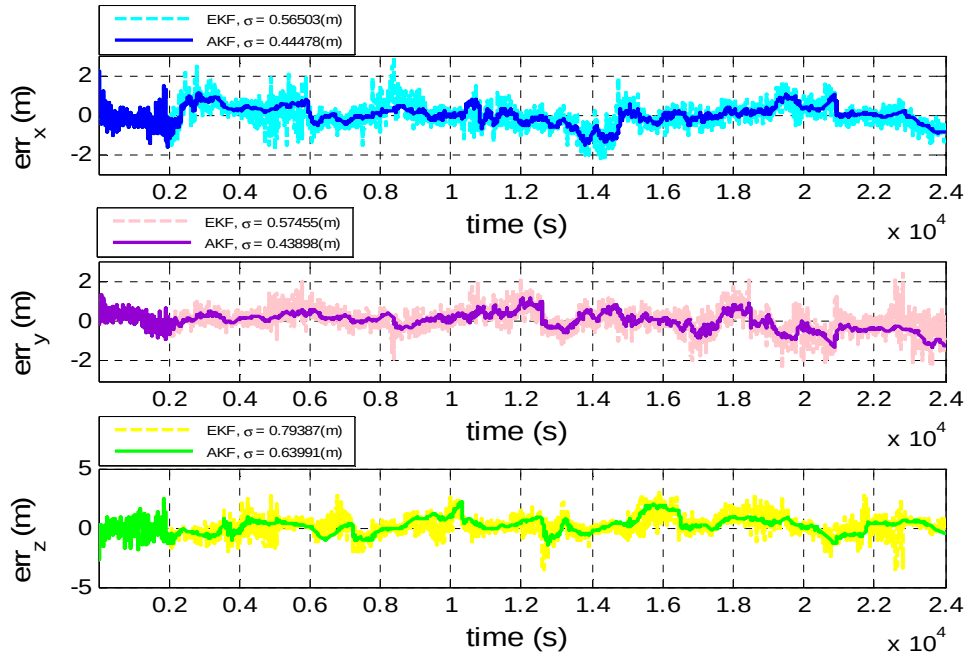

Figure 11. ECEF position error for EKF and AKF computed with $\alpha^{1/2}$=0.02 (2nd scenario).

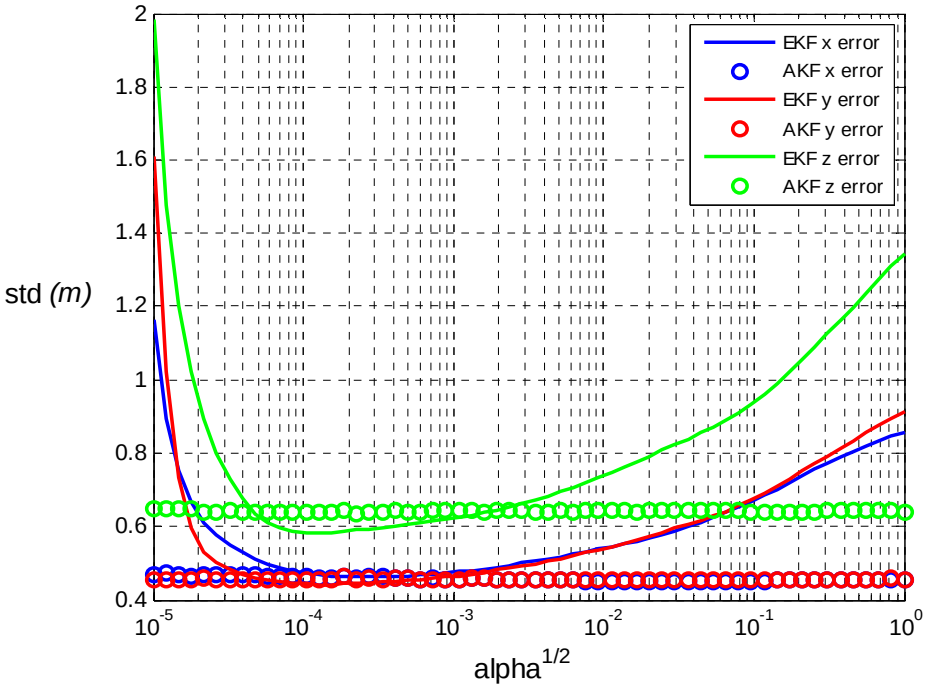

Figure 12. EKF and AKF position error std vs. $\alpha^{1/2}$ value (first guess setting).

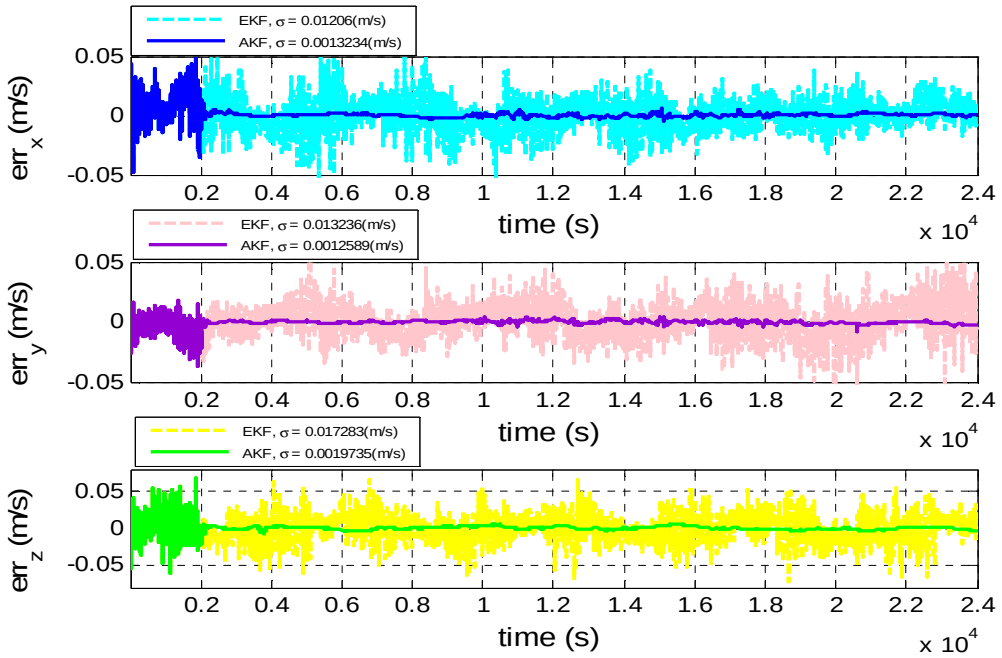

Figure 13. ECEF velocity error for EKF and AKF computed with $\alpha^{1/2}$=0.02 (2nd scenario).

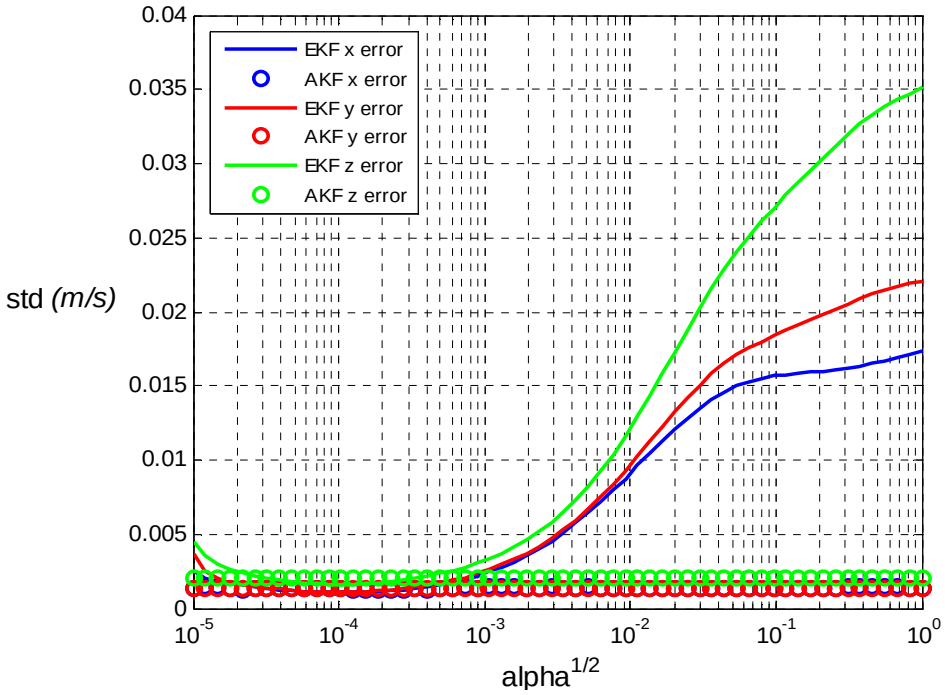

Figure 14. EKF and AKF velocity error std vs. $\alpha^{1/2}$ value (first guess setting)

Scheme Comparison

All the results shown above are obtained by applying the first estimation method - Eq. (17) -. The test on the second scheme - Eq. (18) - has shown that both approaches achieve the same overall performance when the first guess value is over-estimated.

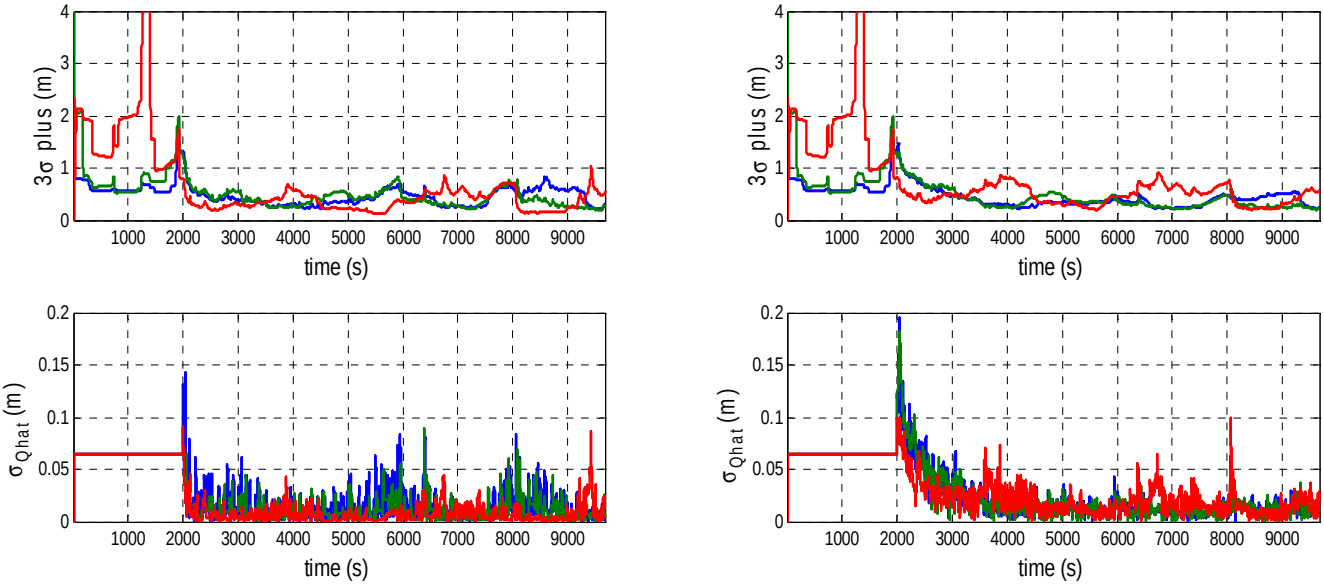

Figure 15. A-posteriori 3σ covariance bound and process noise σ for first (left pictures) and second (right pictures) adaptive estimation scheme (1st scenario dataset). The value refers to x component (blue), y component (red), z component of ECEF position vector.

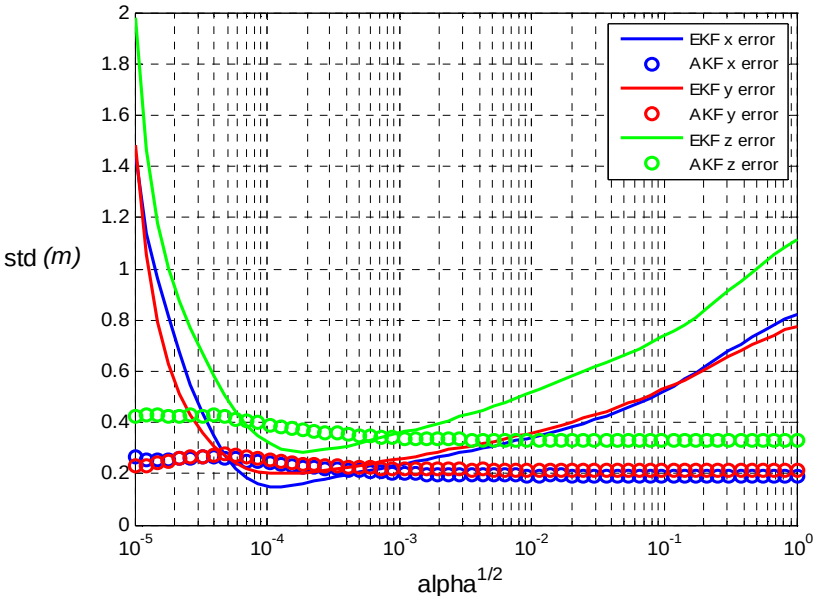

Figure 16. EKF and AKF position error std vs. $\alpha^{1/2}$ value (first guess setting, 1st dataset).

Figure 15 shows the a-posteriori covariance and the estimated process noise for both approaches with $\alpha^{1/2}$=0.02: the process covariance is almost the same and the final filter behavior, represented by the 3σ covariance bound, is preserved.

The comparison of the sensitivity analysis provided in Figure 8 with that one of Figure 16 shows that the second scheme has exhibited a slightly worse precision for small process covariance starting values ($10^{-10} < \alpha < 10^{-8}$).

This behavior is in line with Busse[14], which has already pointed out the worse convergence properties of this estimator for under-estimated first guess sigma values. This limitation should be taken into account during trade-off analysis together with its robustness w.r.t. numerical instability conditions caused by Q values very close to zero.

Window Size Comparison

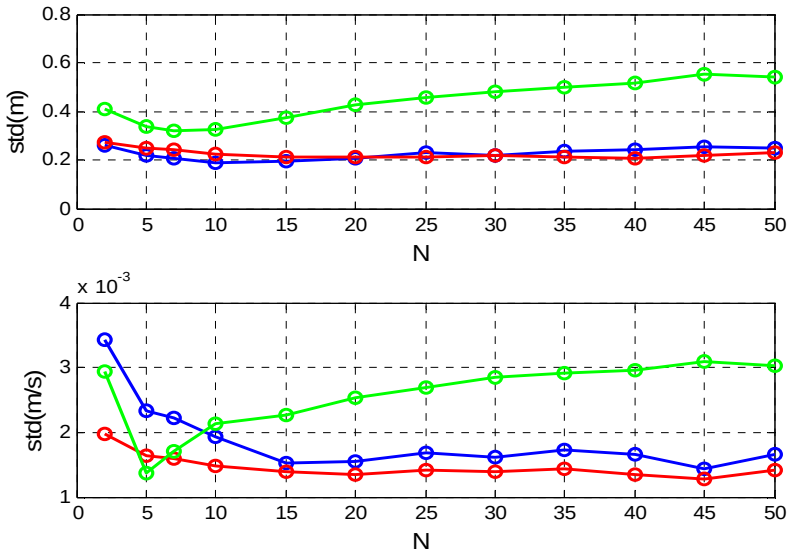

Figure 17. ECEF position and velocity error std vs. adaptive window length ($\alpha^{1/2}$ = 0.02, 1st dataset): x component (blue), y component (red) and z component (green).

One key parameter for a successfully adaptation process is the window length. A large window size could reduce the biases of the estimates but may cause the adaptive filter loosing the capability of adaptation[7]. The window size should be provided by a trade-off evaluation or it can be sized by using off-line optimization algorithm[13].

Figure 17 shows the variation of the adaptive filtering error std w.r.t. the length of the window N for a fixed α value. The first two degrees of freedom are slightly influenced by the window length, so the N=10 chosen length doesn't introduce relevant performance degradation. Instead the third error component, which is subject to the fast dynamics variations, can be improved by reducing the window length, in order to allow a better "interpretation" of disturbances.

More generally, even if the window length influences the final filter performance, it seems to be not critical: the achieved error results are always better than those ones provided by the standard EKF, when it works with a process noise sigma far from the optimal one.

Filter computational load

The following rough estimate of the AKF computational cost for one filter cycle is provided:

$$\left\{3/2\, n^3 + n^2(3p + m/2) + n\,(3/2p + m^2) + p^3\right\} + \left\{n^3\right\} + \left\{nN\right\} \approx 10000 \text{ flop} \qquad (19)$$

where n is the state dimension (8), p is the measurement estimation (16), m is the state process dimension (8) and N is the window length for the adaptive estimation (10).

The first term represents the standard cost of the KF[16], the second and third take into account respectively the evaluation of the integral in Eq. (18) and the moving average window application.

CONCLUSION

A real time POD solution based on an adaptive filtering approach allows to greatly reducing dependency on ground support: filter tuning from analysts during s/c life time is not required anymore.

An AKF solution for this problem has been addressed in this paper. The AKF has been tested and validated by using HIL data provided by a space qualified GPS receiver available on a TAS-I test bench. The AKF has provided the same sub-meter 3D rms performance guaranteed by the optimally tuned EKF devised for real time POD.

A performance analysis has been carried out in order to provide the evidence of the independence of the achievable AKF performance vs. the first guess parameter set (to be loaded on-board). It has also been demonstrated that the window length does not represent a critical point for the filter and that the computational cost is affordable for space qualified processors of LEON3 and upper class.

Further investigation shall be carried out in order to identify the best covariance estimator for guaranteeing robustness. Alternative architectural schemes shall be also explored.

REFERENCES

[1] O. Montenbruck , T. Van Helleputte , R. Kroes , E. Gill, "Reduced dynamic orbit determination using GPS code and carrier measurements", *Aerospace Science and Technology* 9, 2005, pp.261–271.

[2] Goddard Enhanced Onboard Navigation System (GEONS) Mathematical Specifications Version 2, Release 2.13, 2009.

[3] A.C. Long, J.O. Cappellari, C.E. Velez, and A.J. Fuchs, "Goddard Trajectory Determination System (GTDS) Mathematical Theory", National Aeronautics and Space Administration, Goddard Space Flight Center, 1989.

[4] A. Intelisano, L. Mazzini, S. Landenna, A. Zin, L. Scaciga, L. Marradi, " Recent Flight Experiences of TAS-I Onboard Navigation Equipments", *4th ESA Workshop on Satellite Navigation User Equipment Technologies* (NAVITEC-2008).

[5] O. Montenbruck & P. Ramos-Bosch "Precision real-time navigation of LEO satellites using global positioning system measurements" , 10 July 2007, *GPS Solution*, Springer-Verlag GmbH, 2008, Vol. 12, pp. 187–198.

[6] P. Maybeck, "Stochastic models, estimation and control", Vol. 1, New York: Academic Press, 1982.

[7] A. H. Mohamed, K. P. Schwarz, "Adaptive Kalman filtering for INS/GPS", *Journal of Geodesy*. – Heidelberg: Springer-Verlag GmbH, 1999. No. 73, pp. 193–203.

[8] Q. M. Lam, J. L. Crassidis, "Evaluation of a multiple model adaptive estimation scheme for space vehicle's enhanced navigation solution," *Proc. Guidance, Navigation and Control Conference*, AIAA Press, Aug. 2007, AIAA-6816, Hilton Head, SC.

[9] D.J. Jwo, F.C. Chung and T.P. Weng, "Adaptive Kalman Filter for Navigation Sensor Fusion", National Taiwan Ocean University, Sensor Fusion and its Applications, 2010, Ciza Thomas (Ed.).

[10] P. Maybeck, "Stochastic models, estimation and control", Vol. 2, New York: Academic Press, 1982.

[11] A. Almagbile, J. Wang, and W.Ding, "Evaluating the Performances of Adaptive Kalman Filter Methods in GPS/INS Integration", *Journal of Global Positioning Systems*, 2010, Vol.9, No.1, pp. 33-40.

[12] C.F. Von Loan, " Computing Integrals involving Matrix Exponential", *IEEE Transactions on Automatic Control*, Vol. AC-23, No. 3, 1978, pp. 395-404.

[13] H. Lu, J. Zhan-rong, W. Ming-ming, and Z. Li-xin "Adaptive Extended Kalman Filter Based on Genetic Algorithm for Tightly- coupled Integrated Inertial and GPS Navigation", *Intelligent Computation Technology and Automation*, 2009, Vol. 1, Sec. 6, pp. 520-524.

[14] F. D. Busse and J. P. Howy, " Real time experimental demonstration of precise decentralized relative navigation for formation flying spacecraft", *AIAA Guidance, Navigation, and Control Conference*, 2002, Monterey, California.

[15] J. P. How, F. D. Busse, J. Simpson, NASA Goddard Space Flight Center, "Demonstration of Adaptive Extended Kalman Filter for Low Earth Orbit Formation Estimation Using CDGPS", *Journal of the Institute of Navigation*, 2003, Vol. 50, No. 2, pp. 79-93.

[16] M. Verhaegen and P. Van Dooren, "Numerical Aspects of Different Kalman Filter Implementations", *IEEE Transactions on Automatic Control*, Vol. AC-31, No. 10, 1986, pp. 907-917.

[17] W.M. Kaula, "Theory of Satellite Geodesy", Blaisdell publ. Co., Waltham, Mass, 1966.